

# Underwater Acoustic Imaging using Capacitive Micromachined Ultrasonic Transducer Arrays

Ö. Oralkan, A. S. Ergun, C.-H. Cheng, J. A. Johnson, M. Karaman, and B. T. Khuri-Yakub

E. L. Ginzton Laboratory  
Stanford University  
Stanford, CA 94305-4088  
ooralkan@stanford.edu

**Abstract**—Capacitive micromachined ultrasonic transducers (CMUTs) have recently emerged as an alternative technology to piezoelectric transducers, offering advantages such as wide bandwidth, ease of fabricating large arrays and potential for integration with electronic circuits. In this paper, we present 2D and 3D pulse-echo imaging results using 1D linear and 2D rectangular CMUT arrays, respectively. The aim of this paper is to demonstrate the viability of CMUTs for underwater acoustic imaging. For imaging experiments, we have fabricated 1D and 2D CMUT arrays, and built an experimental setup allowing us to transmit and receive ultrasound signals from individual transducer elements. The image quality obtained shows that CMUTs are a strong alternative to conventional piezoelectric transducer arrays for the design of future generations of underwater acoustic imaging systems.

## I. INTRODUCTION

Underwater acoustic imaging systems provide images of underwater objects when water turbidity precludes the use of optical means of viewing. Optical visibility range could be as low as less than a meter. Although the resolution capability of acoustical systems are significantly lower than that of optical systems, acoustical energy can penetrate through muddy waters resulting in a longer imaging range. The applications of underwater acoustic imaging

span a wide variety of disciplines, including commercial (e.g., fishing, underwater construction), scientific (e.g., oceanography, marine biology, archeology) and military (e.g., mine reconnaissance, surveillance, intelligence collection). Some of these applications and related imaging systems are schematically depicted in Fig. 1. The resolution-range tradeoff between optical and acoustical imaging exists between different types of underwater acoustic imaging applications as well [1]. Conventional sonar systems are generally used to determine the locations of underwater objects. These systems are typically employed on surface ships and submarines, and provide long imaging ranges with relatively low resolution due to lower frequencies of operation (e.g., tens of kilohertz). Higher resolution underwater imaging systems are often used to identify an underwater object by gathering information about its geometrical features, rather than only about its location. These systems operate at higher frequencies (e.g., hundreds of kilohertz to a few megahertz) and provide shorter imaging ranges. High resolution underwater imaging systems can be used on unmanned underwater vehicles (UUVs) or as handheld units for divers. Although the specifications for conventional sonar and high resolution systems are different, they share similar hardware implementations and image reconstruction techniques. An emerging underwater imaging modality is 3D imaging using 2D transducer arrays [2]. Two challenges have traditionally limited the feasibility of 3D

This work was supported by the United States Office of Naval Research.

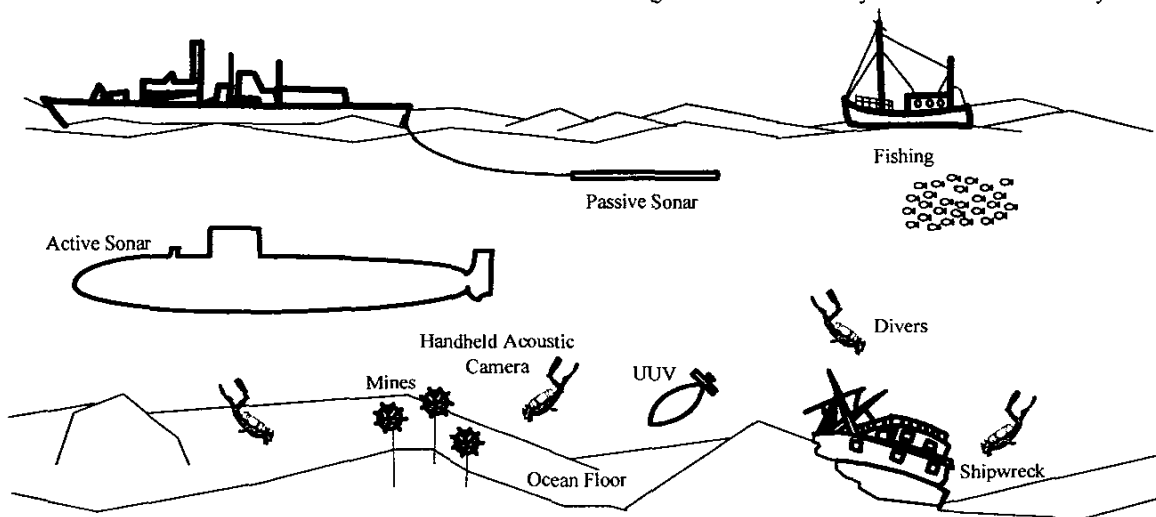


Fig. 1. Schematic representation of underwater imaging applications and related acoustical imaging systems.

## II. CMUT ARRAYS

The basic building block of a CMUT is a capacitor cell consisting of a metalized membrane (top electrode) suspended above a heavily doped silicon substrate (bottom electrode). The membrane is attracted toward the bulk by the electrostatic force, and induced stress within the membrane resists the attraction. Driving the membrane with an alternating voltage generates ultrasound. If the biased membrane is subjected to ultrasound, a current output is generated due to the capacitance change under constant bias voltage. The amplitude of this current output is a function of the frequency of the incident wave, the bias voltage, and the capacitance of the device. 1D and 2D array elements are formed by connecting many capacitor cells in parallel.

### A. 1D CMUT Arrays

The 128-element 1D linear CMUT array used in this study is shown in Fig. 2 along with a 64-element array. Individual capacitor cells constituting the array elements can be seen in the magnified views. For imaging experiments, the 128-element, 1D linear CMUT array was attached and wire bonded onto a printed circuit board (PCB) to provide individual electrical connections to each transducer element. The physical dimensions of the 1D CMUT array used in this work are listed in Table I.

### B. 2D CMUT Arrays

We have designed and fabricated 2D CMUT arrays having as many as 128x128 elements. One of the challenges of using these large 2D arrays is the electrical interconnection allowing transmission to and reception from each individual element. We have developed a scheme to allow flip-chip bonding of these arrays to another layer of circuitry for interconnection, where electrical connection to each element is made possible with a through-wafer via [7]. The via electrically connects the bottom electrode of the CMUT cells in one element to the backside of the wafer. As an experimental prototype, we have successfully mounted a 16x16-element portion of a 32x64-element CMUT array employing through-wafer vias to a glass substrate that provides individual leads from all elements to pads surrounding the array. Although we eventually would like to bond the 2D CMUT array onto a silicon integrated circuit, for initial imaging experiments, we used a glass

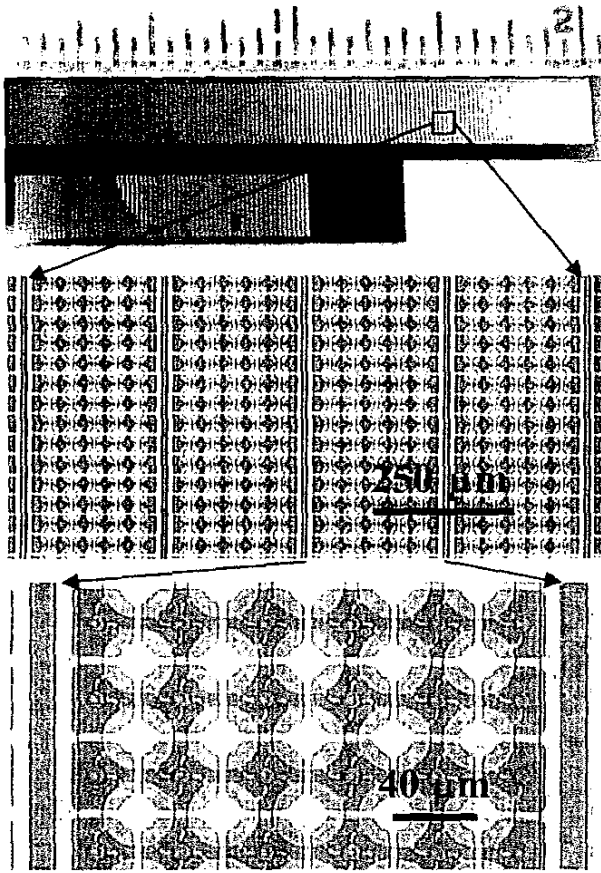


Fig. 2. 128- and 64-element 1D linear CMUT arrays and magnified views of individual elements.

acoustic imaging using 2D arrays: (1) Achieving a sufficiently high acoustic power during transmit and high sensitivity during receive using a small array element, and (2) building and interconnecting dedicated transmit and receive processing circuitry for each element.

CMUTs have recently emerged as an alternative technology to piezoelectric transducers, offering advantages such as wide bandwidth, ease of fabricating large arrays, and potential for integration with electronics [3]. Our group has successfully demonstrated CMUTs operating in the frequency range of 10 kHz to 60 MHz, which spans a wide spectrum of applications from underwater sonar imaging to high-frequency medical imaging [4, 5]. 1D arrays for conventional 2D imaging and 2D arrays with as many as 128x128 elements for real-time volumetric imaging have been fabricated and characterized [6-8].

In this paper, we present immersion imaging results using 1D and 2D CMUT arrays. These results include 2D images from 128-element 1D linear CMUT arrays, and 3D images from 8x16 2D CMUT arrays. The next section describes the 1D and 2D arrays used in this study. Section III describes the experimental setup. The experimental imaging results are presented in Section IV.

TABLE I  
PHYSICAL PARAMETERS OF THE 1D CMUT ARRAY

Number of elements in the array ( $N$ )	128
Length of an element, $\mu\text{m}$	6000
Width of an element, $\mu\text{m}$	200
Element pitch ( $d$ ), $\mu\text{m}$	250
Number of cells in the element	750
Cell diameter ( $d_{\text{cell}}$ ), $\mu\text{m}$	36
Membrane thickness ( $t_m$ ), $\mu\text{m}$	0.9
Gap thickness ( $t_g$ ), $\mu\text{m}$	0.11
Insulating layer thickness ( $t_i$ ), $\mu\text{m}$	0.2
Substrate thickness, $\mu\text{m}$	500

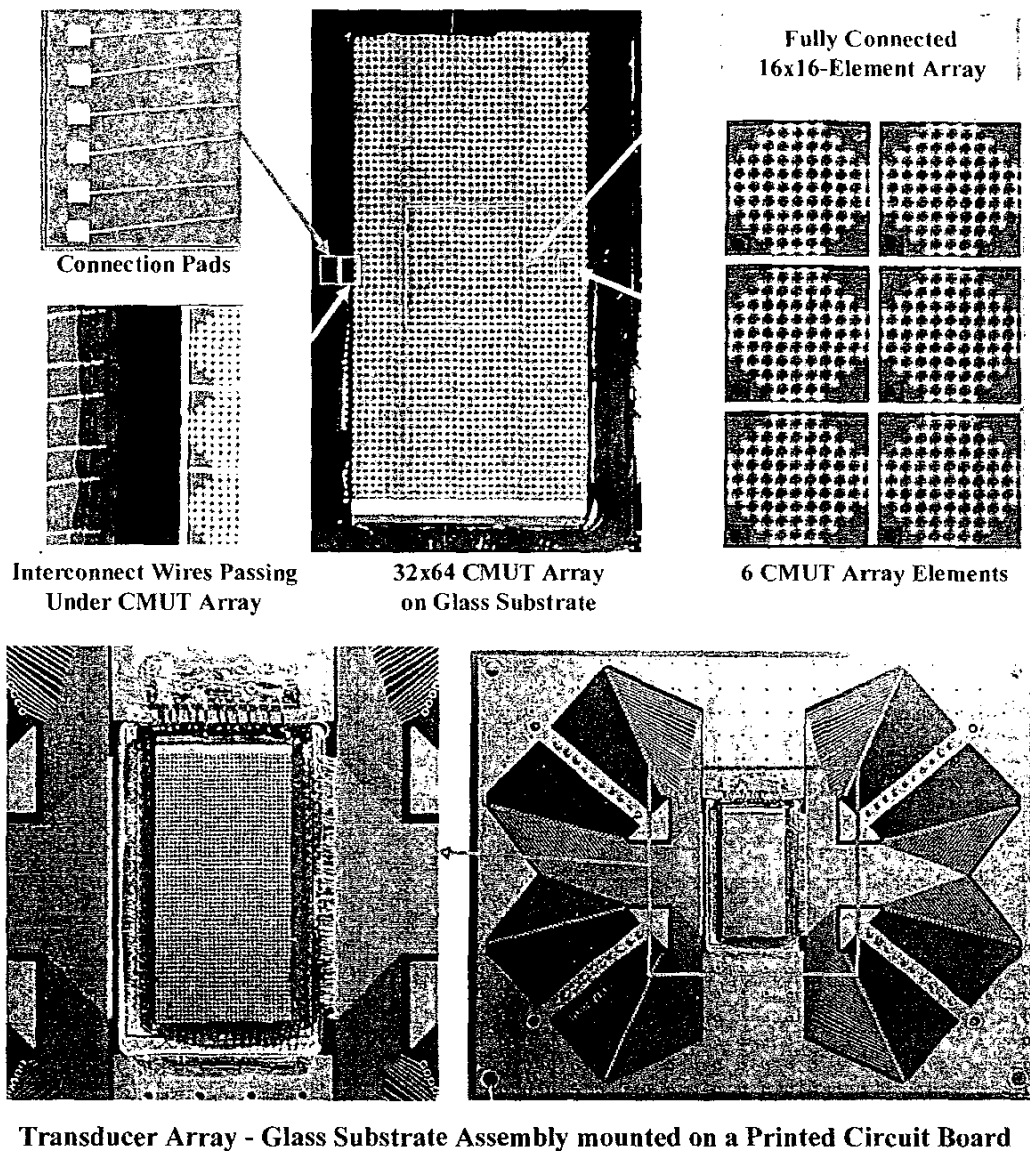


Fig. 3. 2D CMUT arrays and the flip-chip-bonded assembly.

fanout chip that allows us to use the 2D arrays with the experimental setup designed for 1D arrays. The CMUT array-glass substrate assembly is mounted and wire-bonded

onto a PCB. The bonded 2D CMUT array is shown in Fig. 3. The physical dimensions of the 2D CMUT array used in this work are listed in Table II.

TABLE II  
PHYSICAL PARAMETERS OF THE 2D CMUT ARRAY

Element pitch ( $d$ ), $\mu\text{m}$	420
Size of an element, $\mu\text{m}$	$400 \times 400$
Number of cells in the element	76
Cell diameter ( $d_{\text{cell}}$ ), $\mu\text{m}$	36
Membrane thickness ( $t_m$ ), $\mu\text{m}$	0.65
Gap thickness ( $t_g$ ), $\mu\text{m}$	0.1
Insulating layer thickness ( $t_i$ ), $\mu\text{m}$	0.2
Substrate thickness, $\mu\text{m}$	500

### III. EXPERIMENTAL SETUP

The PC-based data acquisition system used in this study included custom designed circuits and a software interface. The experimental setup is shown in Fig. 4. The current system is capable of handling 128 ultrasound channels. For 2D imaging experiments, a 128-element, 1D linear CMUT array was attached and wire bonded onto a PCB to provide individual electrical connections to each transducer ele-

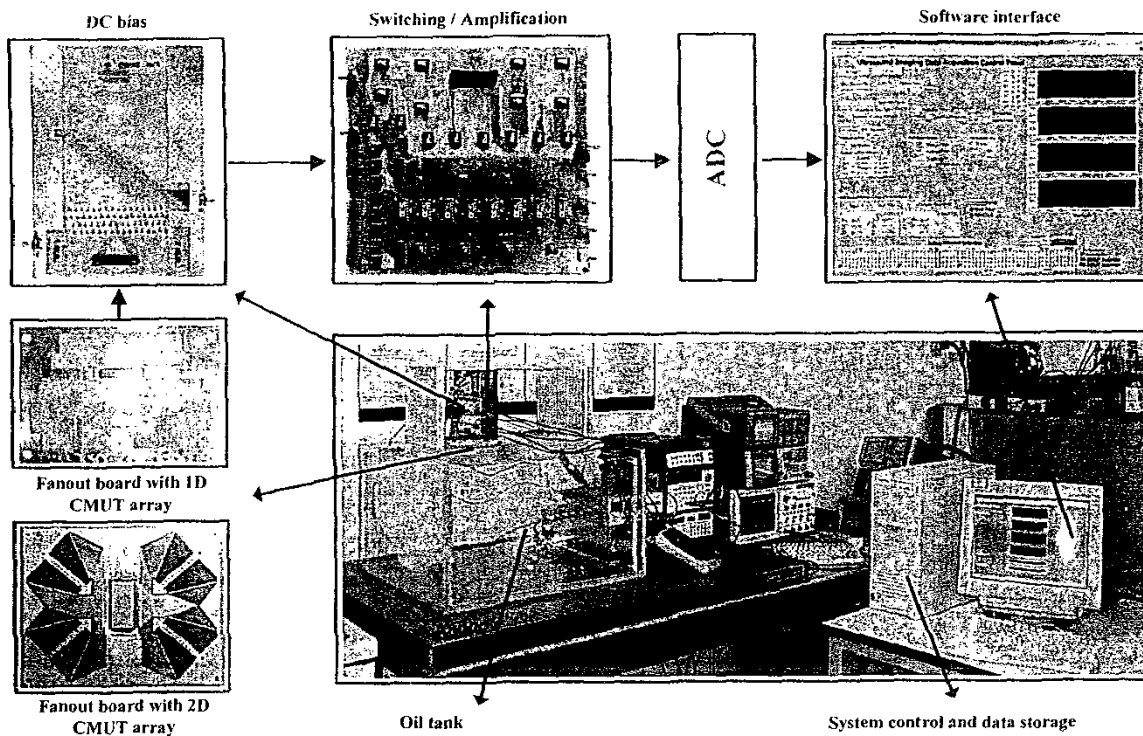


Fig. 4. Experimental setup.

ment. For 3D imaging experiments, half of a 16x16 2D array was used as shown in Fig. 3. The second PCB along the signal path provided the DC bias and AC coupling of transmit and receive signals. A second stage of electronic circuits provided transmit and receive channel selection and amplification of the incoming echo signals. For 2D imaging experiments, the system was used for collecting A-scans from all transmit-receive channel combinations, in which case only one transmit channel and eight receive

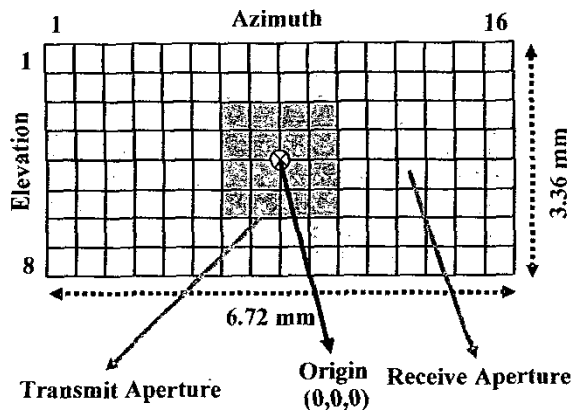
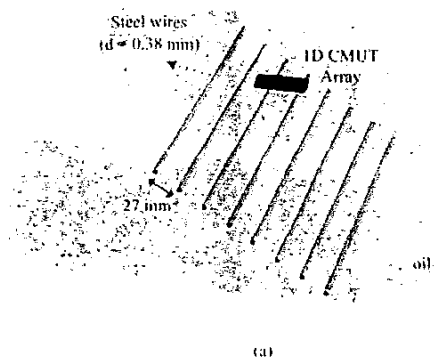


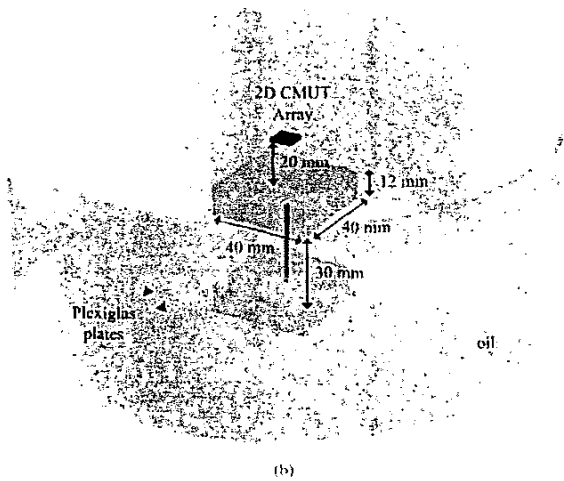
Fig. 5. Array geometry for 8x16 2D CMUT array.

channels were selected at a time. For 3D imaging experiments, in transmit mode, we have used a synthesized powerful virtual element by connecting 4x4 elements (at the center of the 8x16 array) in parallel without any phasing as shown in Fig. 5. The remaining elements in the array were used for receive. A high-voltage DC supply was used to provide the bias voltage for CMUT arrays. A function generator was used for pulsed excitation of the transducer elements. The echo signals were amplified by a fixed gain of 60 dB. The amplified signals were sampled at a rate of 50 MHz and digitized with a resolution of 8-bits. In this experiment, a signal averaging over 100 successive acquisitions was employed to avoid low SNR in A-scans caused by the limited output power of a small number of transducer elements in transmit. The averaged A-scans were stored with a 12-bit sample resolution. The RF A-scans were automatically acquired and stored for offline digital processing.

The imaging phantoms used for 2D and 3D imaging experiments are shown in Fig. 6 (a) and (b), respectively. The 2D resolution test phantom consisted of seven stainless steel wires, each having a diameter of 0.38 mm. The locations of wires were arranged in a diagonal fashion, so that the point spread functions (PSFs) at different spatial locations could be tested. The wire phantom and the CMUT array were immersed in vegetable oil. The 3D imaging phantom consists of two parallel Plexiglas plates, each 12 mm thick and 30 mm apart from each other.



(a)



(b)

Fig. 6. Imaging phantoms. (a) Resolution test phantom for 2D imaging experiments. (b) Parallel-plate phantom for 3D imaging experiments.

## VI. IMAGING RESULTS

### A. 2D Imaging using 1D CMUT Arrays

For 2D imaging experiments, the DC bias voltage on the 1D CMUT array was set to 40 V and a 15-V, 100-ns rectangular pulse was applied to generate ultrasound signals. Fig. 7 shows a sample A-scan. The echo signals coming from seven different wires in the phantom are clearly identified in the figure. This A-scan shows echo signals corresponding to a depth of 210 mm. The amplitude of the echo signals reflected from the first and second wires were smaller than the echo from the third wire because the first two wires in the phantom were located at a larger angle off of the array normal. The lower echo amplitude for these echo signals was a result of the radiation pattern of a single transducer element. The lower amplitude of echo signals for wires beyond the third wire was due to the attenuation in the medium. The pulse-echo frequency response was

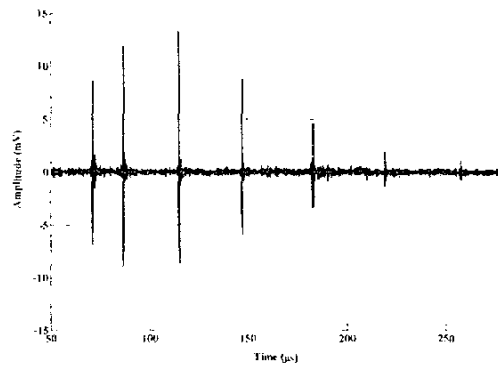
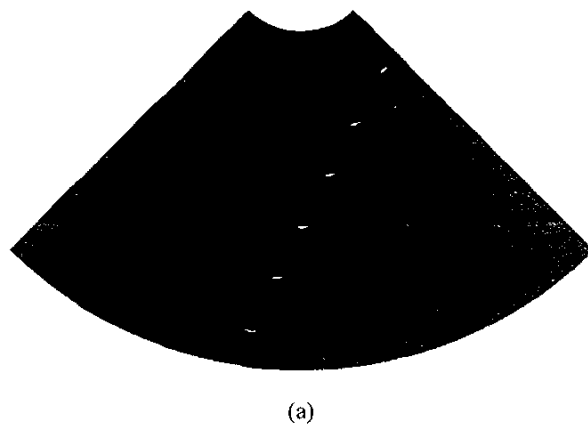
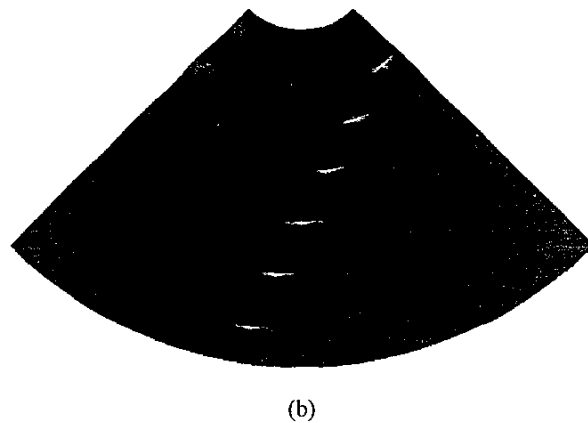


Fig. 7. Sample A-scan from the 1D CMUT array.



(a)



(b)

Fig. 8 The final reconstructed gold standard phased array B-scan sector image with display dynamic range of (a) 40 dB and (b) 60 dB.

found by calculating the Fourier transform of the RF A-scan associated with a single wire. This response was centered at 3 MHz and has a fractional bandwidth of 80% including the effect of the frequency-dependent attenuation. Since the attenuation in water is significantly weaker

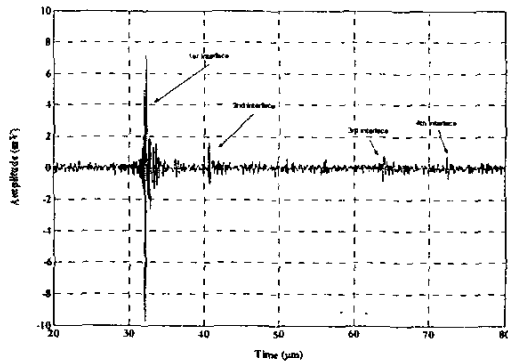


Fig. 9. Sample A-scan from the 2D CMUT array.

than that in vegetable oil, the frequency shaping described is not important in water for short distances. However, one should also note that the imaging range is also significantly longer for underwater imaging. As a result, the attenuation effects should be considered according to frequency of operation chosen and the desired imaging range.

Following the data acquisition, the raw RF A-scan data were processed digitally to reconstruct the images. The images were reconstructed by employing RF beamforming and synthetic phased array approaches [9, 10].

The final reconstructed gold standard phased array B-scan sector image with 210 mm image depth and 90 degrees sector angle is displayed at 40 and 60 dB display dynamic ranges in Fig. 8 (a) and (b), respectively. The image of each wire target represents the PSF of the overall imaging system at that particular location on the imaging plane. The six reflectors identified in the B-scan images correspond to wires 2 to 7 in the phantom. Since the first wire's location is outside the 90-degree sector angle, it does not appear in the resulting images. A grating lobe artifact was observed at a 90 degree angle off of the first and second reflectors. Although the first reflector was not seen in the image, the grating lobe artifact associated with it was visible. The inter-element spacing of the array was 250  $\mu\text{m}$ . This spacing satisfies the  $\lambda/2$  spatial sampling criteria for frequency components up to 3 MHz. Since the CMUT array element had a broadband response, frequency components higher than 3 MHz caused the grating lobe artifact mentioned above. The other signature characteristics of a wide-band system are also present in the resulting images. These include the "bow-tie-like" shape of the 2D PSF and the improved axial resolution due to shorter pulse duration. In the reconstructed images, it was also observed that the electronic noise floor of the image was more than 50 dB below the maximum mainlobe magnitude.

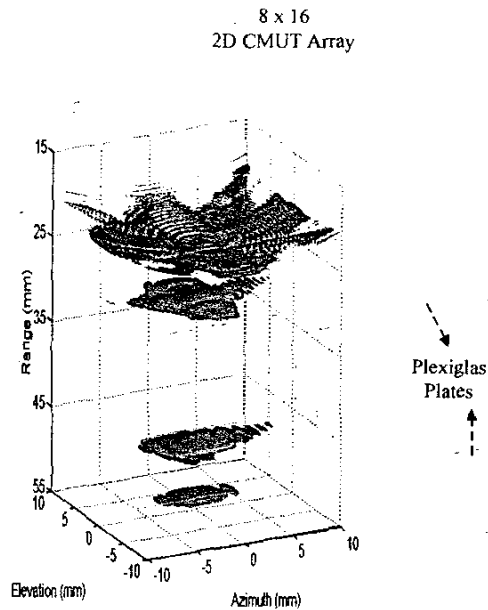


Fig. 10. Surface rendered 3D image of the parallel plate phantom.

### B. 3D Imaging using 2D CMUT Arrays

For 3D imaging experiments, the DC bias voltage on the 2D CMUT array was set to 20 V and a 15-V, 100-ns rectangular pulse was used to excite the 4x4-element unphased transmit subarray at the center of the 8x16 2D array. The remaining elements were used in receive mode. A sample A-scan is shown in Fig. 9.

The 3D image was reconstructed in a similar fashion to the 2D image by employing RF beamforming and synthetic phased array approaches. However, due to the use of a fixed transmit aperture, only dynamic receive beamforming was employed. After the individual voxel values were calculated, a 40 dB logarithmic compression was employed on the volume data and the volumetric image was visualized by surface rendering. This resulting 3D surface rendered image is shown in Fig. 10, where the schematic description of the parallel plate phantom was superimposed on the image. The four oil-Plexiglas interfaces are clearly identified in the image. The azimuthal and elevational cross-sections of the volumetric image are shown in Fig. 11. The display dynamic range of the grayscale cross-sectional images is 40 dB. Although the performance of the experimental system suffered from parasitics due to the use of board-level electronics the image quality obtained was very promising. The integration of transmit-receive electronics with transducer arrays is especially critical for 2D arrays, since the device capacitance itself is very small.

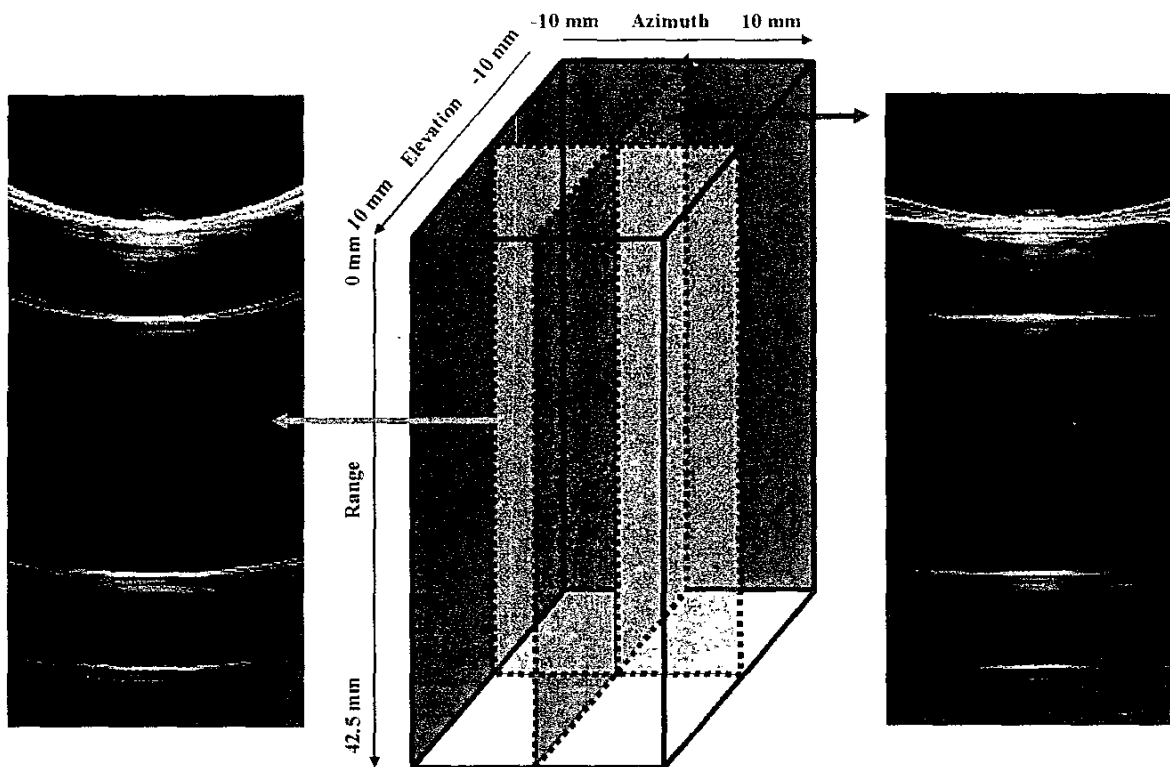


Fig. 11. Azimuthal and elevational cross-sections of the volumetric image.

## V. CONCLUSION

We have previously shown that silicon micromachining can be used to fabricate capacitive ultrasonic transducers that can compete with piezoelectric transducers in terms of efficiency and bandwidth. It is also well known that CMUTs offer easier 1D and 2D array manufacturing and integration with electronic circuitry. In this study, we have presented 2D and 3D pulse-echo imaging results using 1D linear and 2D rectangular CMUT arrays, respectively. The image quality obtained in this study was very promising. We expect that the integration of transmit-receive electronics with transducer arrays, especially 2D arrays, will significantly improve the image quality due to the reduction in parasitics. Based on the results obtained in this study, we strongly believe that CMUTs are a serious contender for the technology of choice in the design and implementation of future underwater acoustic imaging systems.

## REFERENCES

- [1] J. L. Sutton, "Underwater acoustic imaging," *Proc. IEEE*, vol. 67, no. 4, pp. 554-566, April 1979.
- [2] V. Murino and A. Trucco, "Three-dimensional image generation and processing in underwater acoustic vision," *Proc. IEEE*, vol. 88, no. 12, December 2000.
- [3] B. T. Khuri-Yakub, C.-H. Cheng, F. L. Degertekin, S. Ergun, S. Hansen, X. C. Jin, and Ö. Oralkan, "Silicon micro-machined ultrasonic transducers," *Jpn. J. Appl. Phys.*, vol. 39, pp. 2883-2887, May 2000.
- [4] Y. Huang, A. S. Ergun, E. Hægström, M. H. Badi, and B. T. Khuri-Yakub, "Fabrication of Capacitive Micromachined Ultrasonic Transducers (CMUTs) Using Wafer Bonding Technology for Low Frequency (10 kHz-150 kHz) Sonar Applications," *Proc. IEEE Int. Conf. Oceans '02*.
- [5] H. Jagannathan, G. G. Yaralioglu, A. S. Ergun, F. L. Degertekin, and B. T. Khuri-Yakub, "Micro-fluidic channels with integrated ultrasonic transducers," in *Proc. IEEE Ultrason. Symp.*, 2001.
- [6] X. C. Jin, Ö. Oralkan, F. L. Degertekin and B. T. Khuri-Yakub, "Characterization of one-dimensional capacitive micromachined ultrasonic immersion transducer arrays," *IEEE Trans. on Ultrason. Ferroelect. Freq. Contr.*, vol. 48, pp. 750-759, May 2001.
- [7] C.-H. Cheng, E. M. Chow, X. C. Jin, S. Ergun, B. T. Khuri-Yakub, "An efficient electrical addressing method using through-wafer vias for two-dimensional ultrasonic arrays," in *Proc. IEEE Ultrason. Symp.*, 2000, pp. 1179-1182.
- [8] Ö. Oralkan, X. C. Jin, F. L. Degertekin and B. T. Khuri-Yakub, "Simulation and experimental characterization of a 2-D capacitive micromachined ultrasonic transducer array element," *IEEE Trans. Ultrason. Ferroelect. Freq. Contr.*, vol. 46, pp. 1337-1340, Nov. 1999.
- [9] M. Karaman, P.-C. Li, and M. O'Donnell, "Synthetic aperture imaging for small scale systems," *IEEE Trans. Ultrason., Ferroelect., Freq. Contr.*, vol. 42, pp. 429-442, May 1995.
- [10] K. E. Thomenius, "Evolution of ultrasound beamformers," in *Proc. IEEE Ultrasonics Symp.*, 1996, pp. 1615-1622.